Effect of turbostratic disorder in graphitic carbon hosts on the intercalation of lithium

Tao Zheng
Department of Physics, Simon Fraser University, Burnaby, British Columbia, Canada V5A 1S6

J. N. Reimers
Moli Energy (1990) Ltd., 20 000 Stewart Crescent, Maple Ridge, British Columbia, Canada V2X 9E7

J. R. Dahn
Department of Physics, Simon Fraser University, Burnaby, British Columbia, Canada V5A 1S6
(Received 25 July 1994)

The amount of lithium, x_{max}, which can be intercalated in a graphitic carbon host is affected by the amount of turbostratic disorder in the host. Using electrochemical methods, we show that x_{max} in $Li_{x_{max}}C_6$ is given by $x_{max}=1-P$, where P is the probability of finding a random rotation or translation (turbostratic disorder) between adjacent graphite layers, implying that the interlayer spaces or galleries between randomly stacked layers do not host lithium ions. These "blocked " galleries influence the staged phases and the compositions of stage-1 (x_{max}) and stage-2 (x_{2max}) materials. A simple model is proposed to explain the variation of the composition of the stage-2 phase, x_{2max}, with P.

INTRODUCTION

The intercalation of lithium into graphite was discovered in the 1950's.[1] After that, many studies focused on the staged phases[2,3] that are formed during lithium intercalation in graphite and in graphitic carbon types. Safran concluded that the staging phenomenon is the result of the competition between interlayer repulsive and in-plane attractive interactions between the intercalated lithium.[4] Stage-n order is a sequence of n graphite sheets and one intercalate layer as shown schematically in Fig. 1.

Recently, intercalated carbon types and graphites have found application in advanced "lithium-ion" batteries.[5] In such cells, Li_xC_6 is used as the anode and an intercalated transition-metal oxide, like $LiCoO_2$, as the cathode. Developers of such batteries have noticed that the maximum amount of lithium which can be intercalated within the carbon, x_{max}, depends on the crystal structure of the carbon.[6] Furthermore, our own earlier work[7] showed how studies of the electrochemical intercalation of lithium in graphite can be used to determine the phase diagram of Li_xC_6 as a function of x and temperature.

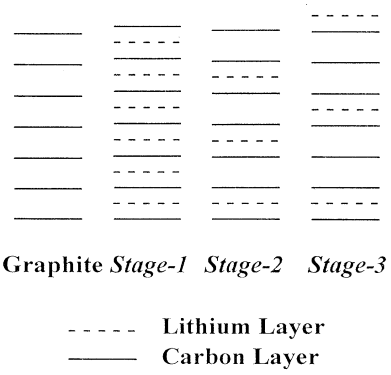

FIG. 1. Schematic diagram of the staged phases of Li intercalated graphite.

As lithium intercalates into graphite a series of staged phases form as x increases. First, there is insertion of lithium into a dilute stage-1 phase, called 1′, followed by a first-order phase transition to a stage-4 phase. For a range of x, the dilute stage-1 and stage-4 phases coexist. In the coexistence region, the chemical potential of lithium in the two phases is equal. Since the voltage of a lithium intercalation cell is given by $V(x)=-\mu(x)/e$, where μ is the chemical potential of the intercalated lithium relative to metallic lithium, plateaus in $V(x)$ are observed in two-phase regions. Figure 2 shows $V(x)$ for a

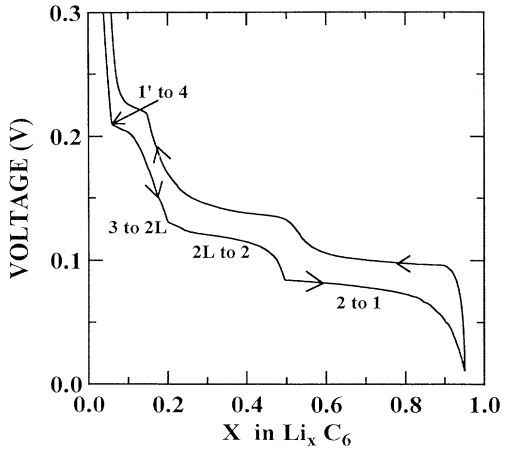

FIG. 2. The voltage profile, $V(x)$, of a Li graphite cell. The graphite used is JMI. The correspondence between the plateaus and the transitions between staged phases has been indicated for the discharge.

lithium/graphite cell, where the two-phase regions have been labeled for the discharge curve following Ref. 7. The transition between stage 2 and concentrated stage 1 is especially easy to observe since it spans a range of almost $\Delta x = \frac{1}{2}$. Electrochemical methods are thus a very sensitive probe of the compositions of the staged phases and the widths of the two-phase regions. In Ref. 6, the staging phase transitions, as probed by measurements of $V(x)$, were shown to be very dependent on the crystal structure of graphitic carbon types.

Franklin carefully studied the microstructure of carbon.[8] She classified all carbon types into two groups: the soft (graphitizing) and the hard (nongraphitizing) carbon types. Soft carbon is almost completely graphitized when heated up to 3000 °C, while hard carbon never becomes graphitized.

In this paper we will consider only the soft carbon types. Soft carbon types are generally produced from aromatic precursors which form a fluid phase during pyrolysis under inert gas. When the heat treatment temperature is limited to about 1000 °C, coke-type materials are formed. These have graphite sheets of relatively small lateral extent (about 20 to 50 Å) which are stacked in a roughly parallel fashion, but with random rotations and translations between every pair of layers. This type of disorder has been given the name "turbostratic disorder."[9] As the carbons are then heated from 1000 to 2000 °C, the lateral extent of the sheets grows and the stacking becomes quite parallel as evidenced by a sharpening of the 002 Bragg peak. However, at 2000 °C there is still complete turbostratic disorder. Upon heating above 2000 °C, the turbostratic disorder is relieved in a more or less continuous way, the amount of remaining turbostratic disorder decreasing to near zero monotonically by 3000 °C.

Recently, Shi and co-workers[10,11] developed a structure refinement program for disordered carbons. The program is ideally suited to studies of the powder-diffraction patterns of soft carbons heated between 2000 and 3000 °C. By performing a least-squares fit between the measured diffraction pattern and a theoretical calculation, parameters of the model structure are optimized. For soft carbon types heated above about 2200 °C, the structure is well described by stacked two-layer packages in AB registry. The stacking of these packages is then performed with the following probabilities: (a) a turbostratic shift or rotation between adjacent packages with probability P'; (b) a registered shift between adjacent packages with probability, P_t', to describe local order $AB/CA/BC$, etc., and (c) no shift between adjacent packages to obtain the stacking $AB/AB/AB$, etc., with probability $(1-P'-P_t')$. Thus, if $P'=0$ and $P_t'=0$, $2H$ graphite is obtained, if $P'=1$ and $P_t'=0$, turbostratic graphite (50%) is obtained, and if $P'=0$ and $P_t'=1$, $3R$ graphite is obtained. It is more convenient to use the stacking probabilities per layer, $P=P'/2$ and $P_t=P_t'/2$, and we will use these below. Shi[11] measured the variation of P and P_t with heat-treatment temperature for a variety of carbon samples.

In this paper we study the insertion of lithium in soft carbon types heated above 2200 °C. Electrochemical methods are used to monitor the composition of the staged phases and the width of the two-phase regions between them. The structure refinement program developed by Shi and co-workers is used to measure the stacking probabilities P and P_t for the carbon samples used. Therefore, we are able to carefully study the effect of stacking disorder on the staging in graphite. We concentrate here on studies of stage 1 and stage 2, leaving higher staged phases for a future work.

EXPERIMENTAL

We used several types of graphitic carbon for this study. These samples are from three different sources. First, mesocarbon microbeads (MCMB) were obtained from Osaka Gas Ltd. This carbon sample had been heat treated to about 1000 °C. We used a Centorr (series 10) graphitizing furnace to further heat the carbons under flowing argon to 2300, 2400, 2500, 2600, 2700, and 2800 °C. Each sample was treated for 1 h at the final temperature. These samples are called MCMB 2300 , . . . , and MCMB 2800, respectively. Second, a petroleum coke sample (type XP, from Conoco, Houston, TX) was heat treated to 2250 and 2300 °C in a similar manner. These samples are called Conoco 2250 and Conoco 2300, respectively. Finally, we studied a commercially available graphite powder (JMI) from Johnson Matthey Inc.

X-ray-diffraction data were collected for each powder sample using a Siemens D5000 powder diffractometer equipped with a copper target tube and a diffracted beam monochromator. The divergence and antiscatter slits were 0.5° and the receiving slit was 0.2 mm for all of our measurements. Samples were held in a rectangular well of dimensions 20 mm × 12 mm × 2.1 mm in a stainless-steel holder. All measurements were made between 10° and 120° in scattering angle.

Electrodes were prepared from the graphitic carbon powders as described previously.[12] First, the carbon powder and 2–5 % by weight of Super S Battery Black (Chemetals Inc. Baltimore, Md) were well mixed with a binder solution to make a viscous slurry. The slurry was then spread in a 100-μm layer on a copper foil substrate. The binder solution was polyvinylidene fluoride dissolved in N-methylpyrolidinone. The amount of binder was adjusted so there would be 2% dead mass in the finished electrodes. The added Super S black reversibly intercalates about $\Delta x = 0.5$ in Li_xC_6.[13] Since only a small amount of Super S black is included in the electrodes, it makes at most systematic error of 2.5% in our determination of x_{max} for a carbon with $x_{max}=1$. We corrected for the effect of Super S black in our work.

Two electrode electrochemical cells of each type of graphitic carbon were constructed using these cathodes. They are all typical lithium coin cells as shown in Fig. 1 of Ref. 6. The electrolyte used here was a 1 mol solution of $LiPF_6$ (Hashimoto) dissolved in a 25:25:50 vol. % mixture of propylene carbonate, ethylene carbonate, and dimethyl carbonate. All cell construction was done in an argon-filled glove box.

All of the cells were tested at 30.0±0.1 °C in a thermostat. The cell cyclers maintained stable currents to

$\pm 1\%$. Changes in x in Li_xC_6 were calculated from the cathode mass, the constant current, and the time of current flow. Data were measured whenever the cell voltage, V, changed by ± 0.001 V in the voltage range between 0.01 and 2.00 V.

RESULTS

Figure 3 shows the changes which occur in the diffraction patterns of the heated MCMB carbon series, and the excellent description of these patterns by the structure refinement program. The structural parameters, P, P_t, a, d_{002}, L_c, and L_a (Ref. 14) for all the carbon samples are listed in Table I.

All cells were tested in the same manner. The first cycle (discharge and charge) of the cells was made using a current which corresponds to a change $\Delta x = 1$ in Li_xC_6 in 50 h. This is called a 50-h rate (for a typical cell with 14-mg active carbon mass, the current is 104 μA). During the first discharge of such a cell an extra plateau near 0.8 V is observed[15] which corresponds to the reaction of electrolyte at the surface of carbon with transferred lithium atoms to form a passivating film. This passivating film is a solid electrolyte[16] and, once formed, prevents further electrolyte reaction. Therefore, this plateau is not observed on subsequent cycles. All careful measurements were made on the second and third cycles of these cells.

The second cycle of the cells was made at a 400-h rate to ensure quasiequilibrium conditions, for examination of the staging transitions. At these small currents, there is an absolute error between the set current and the actual current which varies between channel to channel of our charger system. The currents are stable, but not accurately known. We then cycled all cells a third time, at a 50-h rate, where the currents are accurate to 1% to determine the values of x_{max}. The data measured at the 400-h rate were then normalized to the value of x_{max} determined at the 50-h rate.

Figure 4(a) shows $V(x)$ measured during discharge for a number of carbon samples and Fig. 4(b) shows corresponding data measured during charging. The data shown in Fig. 4 were collected at a 400-h rate. The curves have been sequentially offset by 0.1 V for clarity. Most striking is a reduction of the maximum reversible capacity, x_{max} as P increases. Most of this capacity loss

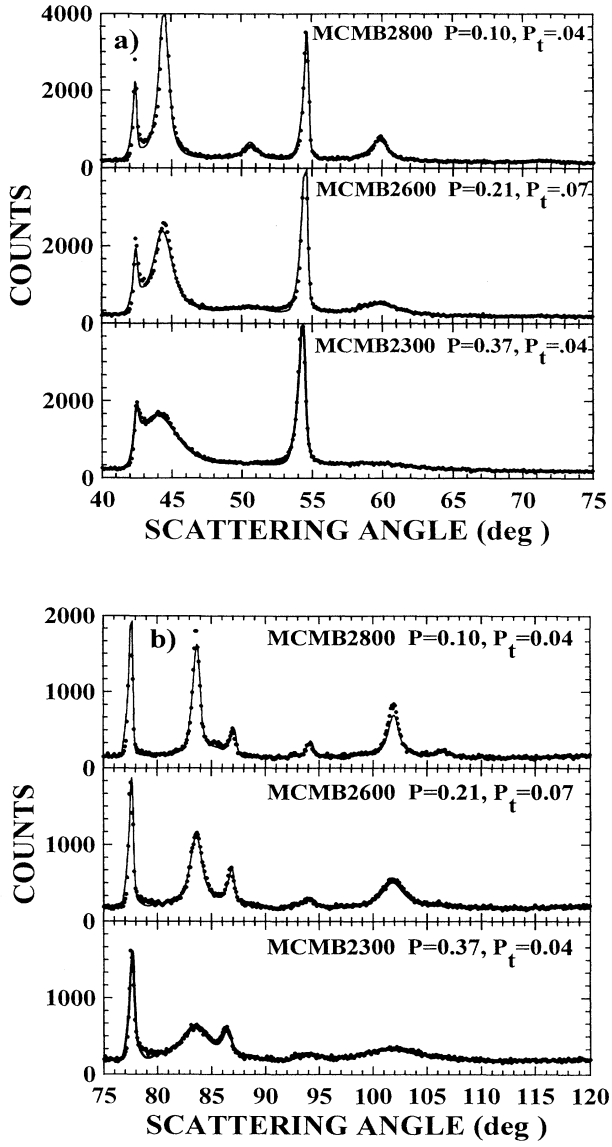

FIG. 3. The x-ray-diffraction patterns (points) and calculated best fits from the structure refinement program (solid lines) for the samples MCMB 2800, 2600, and 2300. (a) 40° ≤ scattering angle ≤ 75°. (b) 75° ≤ scattering angle ≤ 120°.

TABLE I. Structural parameters and capacities (x_{max}, x_{2max}, and x_{21}) for the carbon samples studied.

Name	HTT (°C)	d_{002} (Å)	P	P_t	a (Å)	L_c (Å)	L_a (Å)	x_{max}	x_{2max}	x_{21}
Conoco 2250	2250	3.382	0.42	0.03	2.457	340	294	0.579	0.432	0.147
Conoco 2300	2300	3.376	0.37	0.04	2.457	350	320	0.645	0.457	0.188
MCMB 2300	2300	3.369	0.37	0.04	2.456	440	310	0.657	0.471	0.186
MCMB 2400	2400	3.363	0.29	0.06	2.456	490	310	0.684	0.463	0.221
MCMB 2500	2500	3.359	0.24	0.07	2.456	550	330	0.729	0.454	0.275
MCMB 2600	2600	3.358	0.21	0.07	2.456	560	350	0.788	0.467	0.321
MCMB 2700	2700	3.357	0.17	0.06	2.457	610	360	0.814	0.469	0.346
MCMB 2800	2800	3.352	0.10	0.04	2.457	670	420	0.859	0.473	0.386
JMI	?	3.356	0.05	0.04	2.460	380	330	0.924	0.483	0.441

is due to a shortening of the stage-2–stage-1 plateau.

Figure 5 shows x_{max} plotted versus P for all the carbon types listed in Table I and for many others. There is a linear relationship, well described by $x_{max}=1-P$, which is the straight line in the figure. This implies that little or no lithium is able to intercalate between randomly stacked parallel layers, as we have previously suggested.[6]

Now it is time to analyze the results in Fig. 4 more carefully to learn about the length of the stage-2–stage-1 plateau, x_{21} and the composition of stage-2 phase, x_{2max}. Figure 6 defines these quantities. Figure 7 shows x_{21} and x_{2max} plotted versus P for the carbon samples of Table I and Fig. 4. Also shown is the prediction of the two models to be discussed later. It is clear that x_{2max} remains close to 0.5 independent of P, and that x_{21} is dramatically reduced as P increases. How can this be explained?

The stage-2 phase forms because repulsion between intercalated islands in different layers make the lithium ions move as far apart as possible. When there are no blocked galleries due to turbostratic disorder ($P=0$), the galleries are alternately full (F) and empty (E) as shown in Fig. 8(a). As P increases, x_{max} decreases as $1-P$, sug-

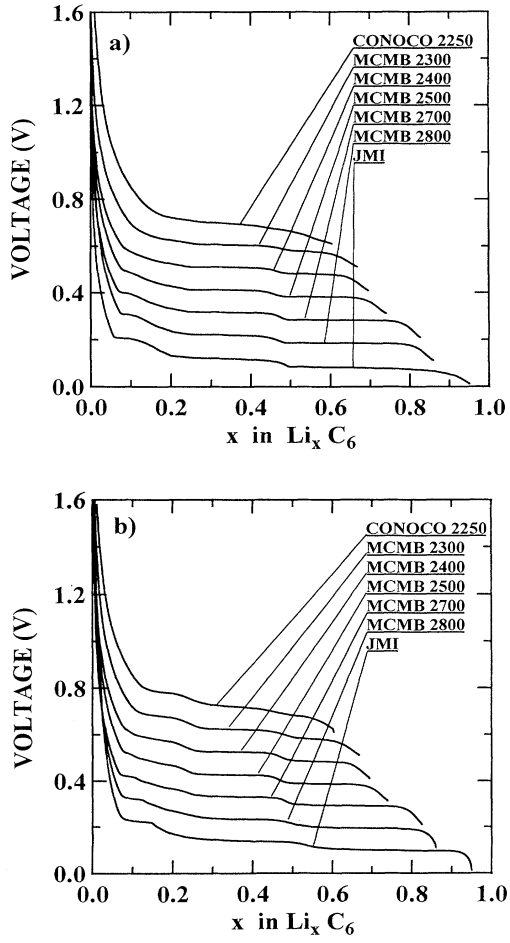

FIG. 4. The voltage profiles of the carbon samples as indicated. The curves have been shifted sequentially by 0.1 V for clarity. (a) Discharge and (b) charge.

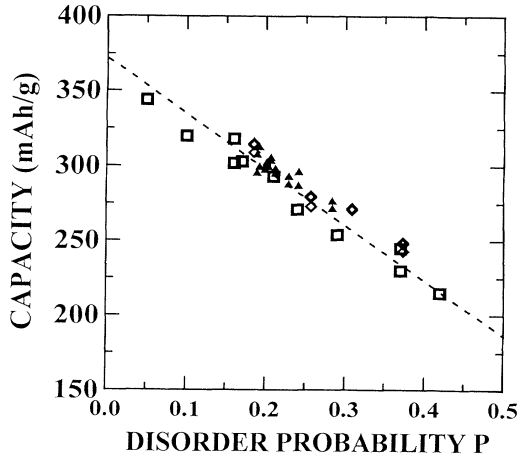

FIG. 5. Capacities versus P for graphitic carbons. □, included in Table I. ◇ and △, other carbon types not included in Table I.

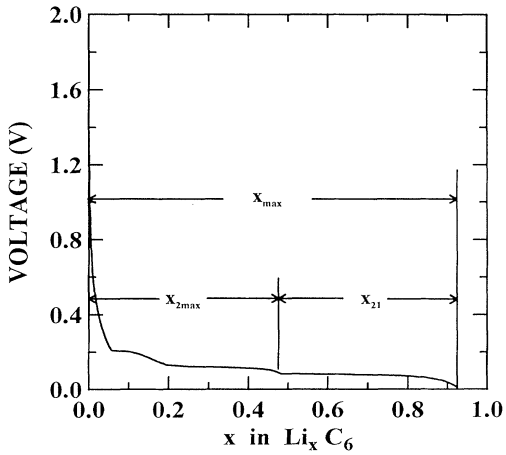

FIG. 6. Schematic showing the definitions of the quantities x_{max}, x_{2max}, and x_{21}.

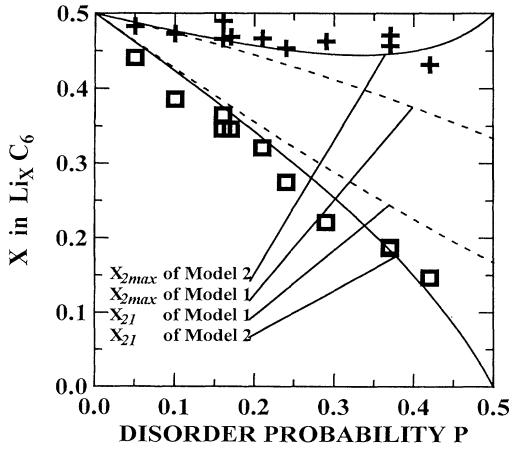

FIG. 7. The variation of x_{2max} and x_{21} with P. Data points are from experiment. Dashed lines are for model 1 and solid lines are for model 2. □, experimental results for x_{21}; +, experimental results for x_{2max}.

MODEL 1 - BLOCKED GALLERIES CAN BE ADJACENT

a)		b)		c)	
F		B		B	
E		F		F	
F		E		E	
E		B		B	
F	P=0.0	F	P=0.33	B	P=0.5
E	x_{2max}=0.5	E	x_{2max}<0.5	F	x_{2max}<0.5
F		F		B	
E		E		F	
F		B		E	
E		B		B	
F		F		B	
E		E		F	

MODEL 2 - BLOCKED GALLERIES NOT ADJACENT

c)		d)		e)	
F		F		F	
E		E		B	
F		B		F	
E		F		B	
F	P=0.0	B	P=0.33	F	P=0.5
E	x_{2max}=0.5	F	x_{2max}<0.5	B	x_{2max}=0.5
F		E		F	
E		F		B	
F		E		F	
E		B		B	
F		F		F	
E		B		B	

F = FULL GALLERY, E=EMPTY GALLERY, B = BLOCKED GALLERY

FIG. 8. Schematic drawing of the stacking given by models 1 and 2 for the stage-2 phase when $P=0.0$, $P=0.33$, and $P=0.5$ as indicated.

gesting that no lithium can be inserted within the galleries between turbostratic layers. We call these galleries blocked and designate them by B. We assume that at the stage-2 composition, full galleries cannot be adjacent. Then, Fig. 8(b) shows the stage-2 composition when $P=0.33$ for blocked galleries which are randomly positioned in the lattice. Figure 8(c) shows the situation for $P=0.5$.

Using a simple model (called model 1) we can predict the dependence of x_{2max} and x_{21} on P. We assume:

(1) $x_{max}=1-P$ and no lithium is allowed in the blocked galleries;

(2) full galleries cannot be adjacent to full galleries;

(3) the amount of lithium in the compound should be maximized subject to condition 2;

(4) blocked galleries are randomly positioned.

Using mathematical induction, and a matrix formalism, we obtain

$$x_{2max}=\frac{1-P}{2-P}$$

and

$$x_{21}=\frac{(1-P)^2}{2-P}=(1-P)-x_{2max}\ .$$

The details of the calculation are given in the Appendix. These expressions are plotted versus P in Fig. 7 as the dashed lines. The agreement is good at small P but poor as P becomes larger.

Since x_{2max} is near $\frac{1}{2}$, even near $P=0.5$, we assumed next, without justification, that perhaps it is impossible for blocked galleries to be adjacent. This would mean that during the thermal treatment of soft carbon above 2000 °C, turbostratic disorder is relieved in such a way that adjacent turbostratic defects are eliminated first, leaving a situation at $P=0.5$ where turbostratic shifts are found between every second set of adjacent layers. Figures 8(d)–8(f) show the stage-2 compositions which would be obtained for $P=0$, $P=0.33$, and $P=0.5$ consistent with the assumption that blocked galleries cannot be adjacent. Notice that $x_{2max}=\frac{1}{2}$ when $P=0.5$ in this case.

We can calculate x_{2max} and x_{21} consistent with these assumptions (called model 2), which are:

(1) $x_{max}=1-P$ and no lithium is allowed in the blocked galleries;

(2) full galleries cannot be adjacent;

(3) blocked galleries cannot be adjacent;

(4) blocked galleries are randomly positioned subjected to condition 3;

(5) the amount of lithium in the compound should be maximized (as many full galleries as possible subject to the above conditions).

We find in this case (see the Appendix),

$$x_{2max}=\frac{(1-P)^2}{2-3P}$$

and

$$x_{21}=(1-P)-x_{2max}=\frac{(1-P)(1-2P)}{2-3P}\ .$$

These expressions are plotted as the solid lines in Fig. 8 and agree well with the data for $0\le P\le 0.4$. This suggests that it is unlikely for blocked galleries to be adjacent.

If blocked galleries cannot be adjacent, then we expect a reasonably well ordered stage-2 structure to form when $P=0.5$ and $x_{21}=0.5$. That is, superstructure peaks should be observable since the spacing between carbon layers bounding full and blocked galleries will differ. Using *in situ* x-ray diffraction,[6] we studied the MCMB 2300 sample ($P=0.37$) carefully in the range near $x=0.5$.

The *in situ* x-ray cell was equilibrated at $V=0.100$ V, corresponding to $x=0.47$ in Fig. 4(b) for the MCMB 2300 charge curve. Figures 9(a) and 9(b) show the (002) peak for the carbon at $2\theta=25.1°$ and the (003) superlattice peak at $2\theta=38.2°$ due to the staged phase. The width of the superlattice peak is $\Delta 2\theta=3°$ which corresponds to a correlation length for the staged order of about 30 Å. If the blocked galleries were randomly arranged, it is unlikely that the correlation length could be so large. Therefore we believe that the blocked galleries tend not to be adjacent. This in turn, implies that turbostratic disorder in graphitic carbon is relieved in an unexpected way. That is, for P less than 0.5, it is unlikely to find two sequential layer pairs both with turbostratic shifts between them.

The structure refinement program for disordered car-

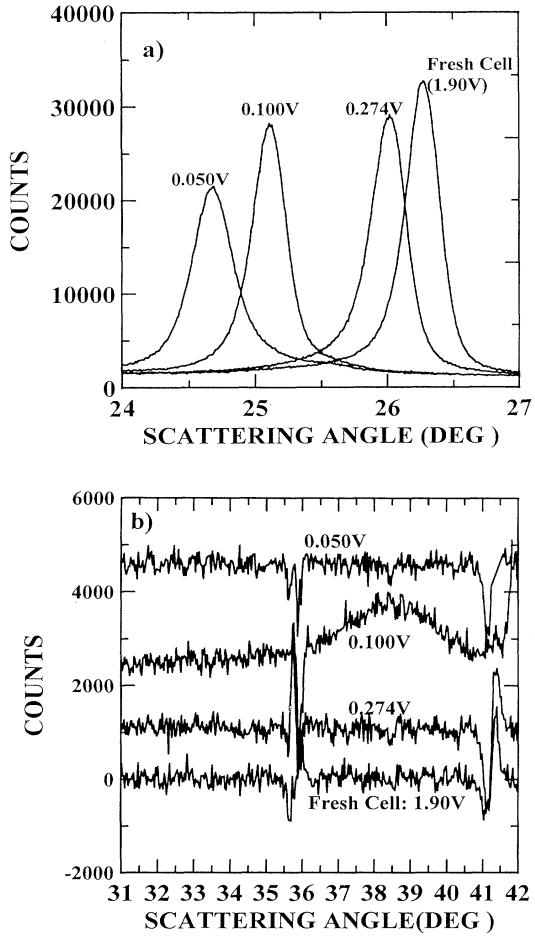

FIG. 9. *In-situ* diffraction results at different voltages for the MCMB 2300 sample. (a) (002) Bragg peak, (b) region of (003) superlattice peak (stage 2). The voltages correspond to the following phases: 1.90 V, no lithium added; 0.274 V, 1′; 0.100 V, stage 2; 0.050 V, stage 1. A second data set measured on the fresh cell has been subtracted from each of the data sets in (b) to reduce the background, and to eliminate peaks from Li (near 36.0°) and BeO (near 41.6°).

bons[10,11] assumes that turbostratic shifts cannot be found between adjacent layer pairs because an *AB* stacked two-layer package is used as the basic unit in the model applicable to high-temperature soft carbon types. Based on our work above, it appears this assumption may be correct and perhaps this is part of the reason for the excellent agreement between the calculation and the data shown in Fig. 3.

DISCUSSION

We have studied the effect of stacking disorder on the intercalation of lithium in soft carbon heated above 2200 °C. We showed:

(1) Lithium is not inserted in the van der Waals space between layers which have a turbostratic shift between them. This conclusion was reached because $x_{\max}=1-P$ was experimentally determined.

(2) The majority of the reduction in $x_{\max}$ with P is caused by a reduction in the length of the stage-2–stage-1 plateau, x_{21}.

(3) The composition of the stage-2 phase, $x_{2\max}$, is weakly dependent on P. This can be explained if blocked galleries cannot be adjacent, which implies that turbostratic disorder is relieved in such a way that turbostratically stacked layers repel one another.

It is not surprising that it is difficult to insert lithium between *parallel* layers which are randomly stacked. When lithium intercalates between *AB* stacked layers, a shift to *AA* stacking occurs.[17] It is likely that the turbostratically stacked layers are pinned by defects (which can only be removed near 2300 °C) preventing the rotation or translation to *AA* stacking. Thus, we can understand why $x_{\max}$ varies as $1-P$, the fraction of layers with *AB* registered stacking.

Lithium intercalation has proved useful in studying stacking disorder in host materials before. In 1984, Dahn and McKinnon[18] showed how careful studies of the order-disorder transition in Li_xTaS_2 by electrochemical methods identified that stacking faults were present between about 10% of adjacent layer pairs. Our result suggesting that turbostratically aligned layer pairs repel one another during the graphitization process is an unexpected result and another example of the use of lithium intercalation as a probe of the disorder in the host.

APPENDIX

1. Development of the model

We develop simple models to describe the stage-2 and stage-1 behavior of lithium intercalation in graphitic carbons. Three reasonable assumptions are made:

(1) $x_{\max}=1-P$ and no lithium in blocked galleries;

(2) full galleries cannot be adjacent;

(3) the amount of lithium in the compound should be maximized subject to condition 2.

Thus, there are only three kinds of galleries in our samples: filled, empty, and blocked galleries. They are labeled *F*, *E*, and *B*, respectively.

To simulate the stacking in our models, we use a matrix method to represent three kinds of galleries:

$$F=(1\ \ 0\ \ 0)\ , \tag{A1}$$

$$E=(0\ \ 1\ \ 0)\ , \tag{A2}$$

$$B=(0\ \ 0\ \ 1)\ . \tag{A3}$$

To introduce the correlation between galleries, two neighboring galleries are considered now. Assume that the probability that F is followed by F is $A_1^{(11)}$; by E is $A_1^{(12)}$; and by B is $A_1^{(13)}$. The probability that E is followed by F is $A_1^{(21)}$; by E is $A_1^{(22)}$; and by B is $A_1^{(23)}$. The probability that B is followed by F is $A_1^{(31)}$; by E is $A_1^{(32)}$; and by B is $A_1^{(33)}$. Hence, the following is always true:

$$A_1^{(m1)}+A_1^{(m2)}+A_1^{(m3)}=1\ ,$$

with $m=1,2,3$.

The correlation between second neighbors can be calculated by multiplying near neighbor correlations. For example, the probability of finding the third gallery filled if the first gallery is filled is

$$A_2^{(11)} = A_1^{(11)} A_1^{(11)} + A_1^{(12)} A_1^{(21)} + A_1^{(13)} A_1^{(31)} .$$

If a 3×3 generation matrix,

$$M = \begin{bmatrix} A_1^{(11)} & A_1^{(12)} & A_1^{(13)} \\ A_1^{(21)} & A_1^{(22)} & A_1^{(23)} \\ A_1^{(31)} & A_1^{(32)} & A_1^{(33)} \end{bmatrix} ,$$

is introduced, the probabilities of finding the first, second, or nth neighbor in a specified state is easily calculated. For example, if the first gallery is filled, multiplying the array (A1) by M will give the probabilities for the type of the second gallery, multiplying by M^2 will give the third gallery, . . . , and by M^n will give the $(n+1)$th gallery. The probabilities for the nth gallery to be filled, empty, or blocked if the first gallery is filled are represented by the elements of the first row in the matrix M^{n-1}, $A_{n-1}^{(11)}$, $A_{n-1}^{(12)}$, and $A_{n-1}^{(13)}$, respectively. So, the probability of finding filled galleries in an n-layer sample is

$$\left[\frac{1}{n}\right] \sum_n A_{n-1}^{(11)} ; \tag{A4}$$

the probability of finding empty galleries is

$$\left[\frac{1}{n}\right] \sum_n A_{n-1}^{(12)} ; \tag{A5}$$

and the probability of finding blocked galleries is

$$\left[\frac{1}{n}\right] \sum_n A_{n-1}^{(13)} , \tag{A6}$$

for large n (approaching ∞). In fact, the results of (A4)–(A6) are the measurables $x_{2\max}$, x_{21}, and P, respectively. Two models are developed next to simulate the compositions of stage 2 and stage 1.

2. Model 1

A random distribution of blocked galleries is assumed (refer to Fig. 8). Consider two consecutive galleries labeled A and B. We assume, if A is filled, there will be probability P'' for B to be blocked and a probability $(1-P'')$ for B to be empty. If A is empty, there will be probability P'' for B to be blocked and a probability $(1-P'')$ for B to be filled. If A is blocked, there will be probability P'' for B to be blocked and a probability $(1-P'')$ for B to be filled. Then the generation matrix M is

$$\begin{bmatrix} 0 & 1-P'' & P'' \\ 1-P'' & 0 & P'' \\ 1-P'' & 0 & P'' \end{bmatrix} .$$

If we take an infinite layer model, the probability of finding a blocked gallery is

$$P = P'' .$$

The capacities $x_{2\max}$ and x_{21} can be calculated from (A4) and (A5), giving

$$x_{2\max} = \frac{1-P}{2-P} ,$$

$$x_{21} = \frac{(1-P)^2}{2-P} .$$

The results of model 1 for $x_{2\max}$ and x_{21} are presented in Fig. 7 and compared to experimental data. This model does not work well.

3. Model 2

Blocked galleries can not be adjacent (refer to Fig. 8). Consider two consecutive galleries labeled A and B. If A is filled, there will be probability P'' for B to be blocked and a probability $(1-P'')$ for B to be empty. If A is empty, there is a probability P'' for B to be blocked and a probability $(1-P'')$ for B to be filled. If A is blocked, the layer B is always filled. Hence, the generation matrix is

$$M = \begin{bmatrix} 0 & 1-P'' & P'' \\ 1-P'' & 0 & P'' \\ 1 & 0 & 0 \end{bmatrix} .$$

The probability P to find a blocked gallery is

$$\frac{P''}{1+P''} = P .$$

Using Eqs. (A4) and (A5) we find

$$x_{2\max} = \frac{1}{(1+P'')(2-P'')} = \frac{(1-P)^2}{2-3P} ,$$

$$x_{21} = \frac{1-P''}{(1+P'')(2-P'')} = \frac{(1-P)(1-2P)}{2-3P} .$$

In Fig. 7, the results of model 2 for $x_{2\max}$ and x_{21} are compared to the experimental data. The results fit the data well.

[1]A. Herold, Bull. Soc. Chim. Fr. **187**, 999 (1955).
[2]J. E. Fischer, in *Chemical Physics of Intercalation*, edited by A. P. LeGrand and S. Flandrois (Plenum, New York, 1987), p. 59.
[3]M. S. Dresselhaus and M. Endo, in *Graphite Intercalation Compounds II*, edited by H. Zabel and S. A. Solin (Springer-Verlag, Berlin, 1992), p. 347.
[4]S. A. Safran, Phys. Rev. Lett. **44**, 937 (1980).
[5]T. Nagaura and K. Tozawa, Prog. Batteries Sol. Cells **9**, 209 (1990).
[6]J. R. Dahn, A. K. Sleigh, Hang Shi, J. N. Reimers, Q. Zhong, and B. M. Way, Electrochim. Acta **38**, 1179 (1993).
[7]J. R. Dahn, Phys. Rev. B **44**, 9170 (1991).
[8]R. E. Franklin, Acta Crystallogr. **4**, 253 (1951); **3**, 107 (1950); **3**, 158 (1950); Proc. R. Soc. London Ser. A **209**, 196 (1951).
[9]B. E. Warren, Phys. Rev. B **9**, 693 (1941).

[10]Hang Shi, J. N. Reimers, and J. R. Dahn, J. Appl. Crystallogr. **26**, 827 (1993).
[11]Hang Shi, Ph.D. thesis, Simon Fraser University, 1993.
[12]J. R. Dahn, R. Fong, and M. J. Spoon, Phys. Rev. B **42**, 6424 (1990).
[13]Z. X. Shu, R. S. McMillan, and J. J. Murray, J. Electrochem. Soc. **140**, L101 (1992).
[14]K. Kinoshita, *Carbon, Electrochemical and Physicochemical Properties* (Wiley, New York, 1988).
[15]R. Fong, U. von Sacken, and J. R. Dahn, J. Electrochem. Soc. **137**, 2009 (1990).
[16]E. Peled, J. Electrochem. Soc. **126**, 2047 (1979).
[17]R. C. Boehm and A. Banerjee, J. Chem. Phys. **96**, 1150 (1992).
[18]J. R. Dahn and W. R. McKinnon, J. Phys. C **17**, 4231 (1984).